Giant vortex dynamics in confined bacterial turbulence

Giant vortex dynamics in confined bacterial turbulence

L. Puggioni,[1] G. Boffetta,[1] and S. Musacchio[1,*]

[1] *Dipartimento di Fisica and INFN, Università degli Studi di Torino, via P. Giuria 1, 10125 Torino, Italy.*

(Dated: January 10, 2023)

We report the numerical evidence of a new state of bacterial turbulence in confined domains. By means of extensive numerical simulations of the Toner-Tu-Swift-Hohenberg model for dense bacterial suspensions in circular geometry, we discover the formation a stable, ordered state in which the angular momentum symmetry is broken. This is achieved by self-organization of a turbulent-like flow into a single, giant vortex of the size of the domain. The giant vortex is surrounded by an annular region close to the boundary, characterized by small-scale, radial vorticity streaks. The average radial velocity profile of the vortex is found to be in agreement with a simple analytical prediction. We also provide an estimate of the temporal and spatial scales of a suitable experimental setup comparable with our numerical findings.

INTRODUCTION

Flowing active matter is one of the most fascinating examples of out-of-equilibrium systems which sits at the intersection between statistical physics, biophysics and fluid dynamics [1–3]. In dense active systems, such as suspensions of bacteria, the collective motion of the individual swimmers produces complex flows at scales much larger than the single swimmer [4, 5], often with chaotic dynamics on several length scales [6–10]. In these conditions, the flow produced by the swimmers has several similarities with usual, high Reynolds number turbulence, including the presence of coherent structures [11–14], a wide range of active scales and anomalous transport [15, 16] and it leads to states called active turbulence [3].

In order to understand and rationalize the experimental observations, a considerable theoretical effort has been devoted to develop continuous, coarse-grained descriptions of dense active suspensions [17–20]. More recently, simple models with a reduced number of parameters have been introduced [12, 21–25], and compared with experimental results [12, 26–28]. These minimal models reproduce several features of active turbulence such as spontaneous flow [29, 30] and multiscale dynamics [31–34], clustering [35, 36] and anomalous diffusion [37].

The numerical studies of these models are often performed in two-dimensions. This is motivated by the fact that most of the experiments of bacterial suspensions are conducted in quasi-two-dimensional domains. Moreover, periodic boundary conditions are often assumed since one is interested in the bulk properties of the active flow. Nonetheless, experiments have shown that confining boundaries can play an important role in the organization of the flow, inducing the emergence of various forms of coherent structures in different types of active fluids [5, 38–42]. In particular, recent experimental studies have shown that confining the bacterial suspension in circular micro-wells induces the formation of a rectified vortex [5, 43, 44].

Here we pursue the investigation of the importance of boundaries by presenting the results of extensive numerical simulations of the Toner-Tu-Swift-Hohenberg (TTSH) model [12, 26] confined in two-dimensional circular domains. We show that the geometrical confinement induces the transition to a novel regime, characterized by the formation of a giant vortex surrounded by an annular region of elongated vorticity structures (streaks). This state has larger size and different velocity profile with respect to the vortical structures reported in previous studies [5, 43, 45] and it originates from a different process which involves complex interactions between the chaotic flow and the boundaries. By an exploration of the parameter space we find that the appearance of the giant vortex is a robust feature of the model in the presence of confinement, and it occurs in a range of physical parameters accessible to experiments of bacterial turbulence.

TONER-TU-SWIFT-HOHENBERG MODEL

The equation for the coarse-grained collective velocity field $\boldsymbol{u}$ of bacterial suspensions in the TTSH model takes the form

$$\partial_t \boldsymbol{u} + \lambda \boldsymbol{u} \cdot \boldsymbol{\nabla} \boldsymbol{u} = -\boldsymbol{\nabla} p - (\alpha + \beta |\boldsymbol{u}|^2 + \Gamma_2 \nabla^2 + \Gamma_4 \nabla^4) \boldsymbol{u} \, . \tag{1}$$

The pressure gradient $\boldsymbol{\nabla} p$ ensures the incompressibility of the flow, $\boldsymbol{\nabla} \cdot \boldsymbol{u} = 0$, which is valid for dense suspensions. The parameters $\lambda, \alpha, \beta, \Gamma_2, \Gamma_4$ are determined by the properties of the microswimmers. For pusher swimmers one has $\lambda > 1$, while $\lambda < 1$ corresponds to pullers [3]. The Swift-Hohenberg operator $\Gamma_2 \nabla^2 + \Gamma_4 \nabla^4$ selects the characteristic scale $\Lambda = 2\pi\sqrt{2\Gamma_4/\Gamma_2}$ at which the flow is forced by the microscopic motion [46]. For $\alpha < 0$, the Landau force $(\alpha + \beta |\boldsymbol{u}|^2)\boldsymbol{u}$ promotes the formation of collective motion with velocity $U = \sqrt{-\alpha/\beta}$. Larger values of $|\alpha|$ correspond to stronger aligning interactions between the swimmers, as in the original Toner-Tu (TT) model for flocking [47, 48]. The TTSH model displays a very rich phenomenology which is the subject of an intense research activity [31, 49–52]. Generalizations of the TTSH model to include coupling with a fluid velocity field and compressible flows have been proposed [35, 53, 54]. We remind that the TTSH model has been developed as a model for bacterial suspensions. Therefore, the results presented in the following are not generalizable to other active systems such as cytoskeletal filaments and molecular motors.

THE RISE OF THE GIANT VORTEX

We performed a set of numerical simulations of the TTSH model confined in two-dimensional circular domains of radius R. No-slip boundary conditions are imposed at the border of the circular domain by means of the penalization

method [55], by adding the term $-\frac{1}{\tau}\mathcal{M}(r)\boldsymbol{u}$ to the r.h.s. of (1) where τ represents the permeability time and is the smallest dynamical time in the system. The mask function $\mathcal{M}(r) = (\tanh((r-R)/(2\Delta x)) + 1)/2$ imposes a sharp decay of the fields at the boundary on a scale of few grid points with spacing Δx. Numerical integration of (1) supplemented with the penalization term is obtained by fully dealiased pseudospectral code with fourth-order Runge Kutta time scheme. The parameters of the simulations are reported in Table I.

	R	N^2	α
A1	16Λ	512×512	-2.00
A2			-1.75
A3			-1.50
A4			-1.25
B1	23Λ	1024×1024	-2.00
B2			-1.75
B3			-1.50
C1	31Λ	1024×1024	-2.00
C2			-1.75
C3			-1.50

TABLE I: Values of coefficient α, confinement radius R and numerical resolution N^2, for the three sets of simulations (A, B, C). All the simulations are performed with parameters $\lambda = 3.5$, $\beta = 0.01$, $\Gamma_2 = 2$, $\Gamma_4 = 1$, $\tau = 0.001$, and grid spacing $\Delta x = 5/64\Lambda$.

For the analysis, we decompose the velocity field in the radial and angular components $\boldsymbol{u} = u_r\hat{\boldsymbol{r}} + u_\varphi\hat{\boldsymbol{\varphi}}$ which define the radial and angular kinetic energies $E_r = \frac{1}{2}\langle u_r^2\rangle$ and $E_\varphi = \frac{1}{2}\langle u_\varphi^2\rangle$ (here and in the following, $\langle\cdot\rangle$ denotes spatial average over the circular domain of radius R).

We let the system evolve starting form a null velocity field seeded with an infinitesimal random perturbation. At the beginning of the simulation, the swimmers organize in a large number of small-scale vortices, with equal probability of positive and negative vorticity and homogeneous and isotropic spatial distribution. In this stage, the statistical properties of the flow are identical to those observed in simulations with periodic boundary conditions [31, 32]. After a short time, the system evolves towards an intermediate, turbulent-like regime, characterized by the presence of multiple large-scale vortices, which move chaotically and are surrounded by regions of vorticity streaks (see Fig. 1, left panel).

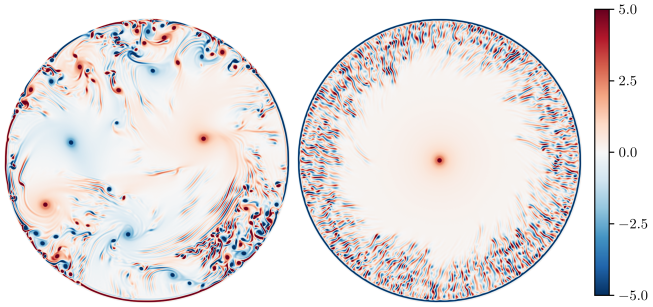

FIG. 1: Vorticity field for the simulation with $R = 31\Lambda$ and $\alpha = -1.75$ at $t = 210\Lambda/U$ (left) and $t = 550\Lambda/U$ (right).

During this stage of the simulation we observe equipartition (with strong temporal fluctuations) between the radial and angular components of the kinetic energy (see Fig. 2). At later times, the system displays a rapid increase of E_φ accompanied by the decrease of E_r, which indicates the transition to a novel regime characterized by $E_\varphi \simeq E_0 \equiv \frac{1}{2}U^2$ and $E_r \simeq 0$. This corresponds to the self-organization of the swimmers in a state of *circular flocking*, that is, a stationary, single, giant vortex which spans the whole domain (see Fig. 1 right panel), similar to that observed in experiments of bacterial suspension in a viscoelastic fluid [56].

The formation of this large-scale structure causes a symmetry breaking of the angular momentum of the flow $M = \langle \boldsymbol{r} \times \boldsymbol{u}\rangle$. As shown in Fig. 3, the values of M fluctuate around zero before the formation of the giant vortex. Later, M saturates to a constant value $|M| \simeq M_0 \equiv \frac{2}{3}UR$ with definite sign. Changing the initial condition of the flow, we observed a strong variability of the transition times from the intermediate turbulent regime to the giant-vortex state (see the inset of Fig. 3).

In Figure 4 we compare the energy spectra $E(k)$ before and after the transition (the spectra correspond to the fields

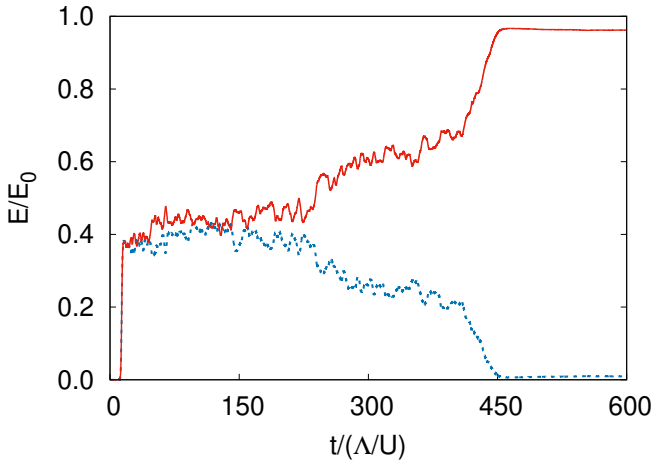

FIG. 2: Temporal evolution of the radial and angular components of the kinetic energy E_r (blue, dashed line), E_φ (red, solid line) normalized with $E_0 = \frac{1}{2}U^2$.

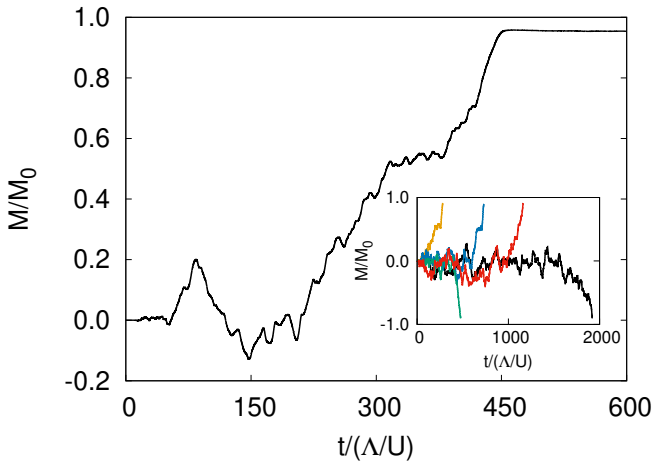

FIG. 3: Temporal evolution of the angular momentum M normalized with $M_0 = \frac{2}{3}UR$ for the simulation at $R = 31\Lambda$ and $\alpha = -1.75$. The inset shows the evolution of the angular momentum for an ensemble of simulation with different initial conditions with $\alpha = -1.50$ and $R = 16\Lambda$.

shown in Figure 1). Before the transition, we find that the intermediate regime is characterized by a turbulent-like power-law energy spectrum $E(k) \sim k^{-\zeta}$, similar to what observed in recent numerical simulations of the TTSH model with periodic boundary conditions [57], although the spectral slope $\zeta \simeq -2$ observed in our simulations is steeper than the value $-3/2$ reported in [57]. After the formation of the giant vortex, we observe a spectral condensation of the energy in the lowest mode, accompanied by a depletion of the energy spectrum at intermediate wavenumbers. At wavenumbers $k \gtrsim 2\pi/\Lambda$ the spectrum remains almost unchanged.

The degree of order of the collective motion of the swimmers in the giant vortex can be quantified by the vortex order parameter [5, 43, 44] which is defined as $\Phi = (\langle|\boldsymbol{u}\cdot\hat{\boldsymbol{\varphi}}|\rangle/\langle|\boldsymbol{u}|\rangle - 2/\pi)/(1-2/\pi)$. A velocity field oriented in the angular direction $\boldsymbol{u} \parallel \hat{\boldsymbol{\varphi}}$ gives $\Phi = 1$, while $\Phi = 0$ corresponds to random-oriented velocity. The values of Φ measured in the late stage are very close to 1, (see Figure 5), which indicates that the motion of the swimmers is highly ordered. The degree of order increases reducing the radius R of the domain and increasing $|\alpha|$.

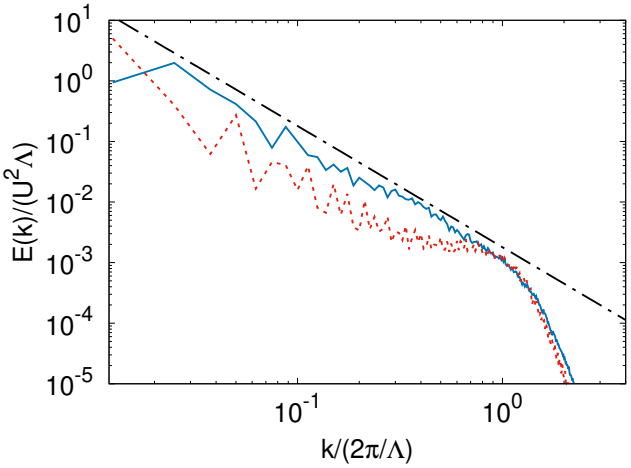

FIG. 4: Energy spectra for the simulation with $R = 31\Lambda$ and $\alpha = -1.75$ at $t = 210\Lambda/U$ (blue, solid line) and $t = 550\Lambda/U$ (red, dashed line). The black, dash-dotted line represents the slope k^{-2}.

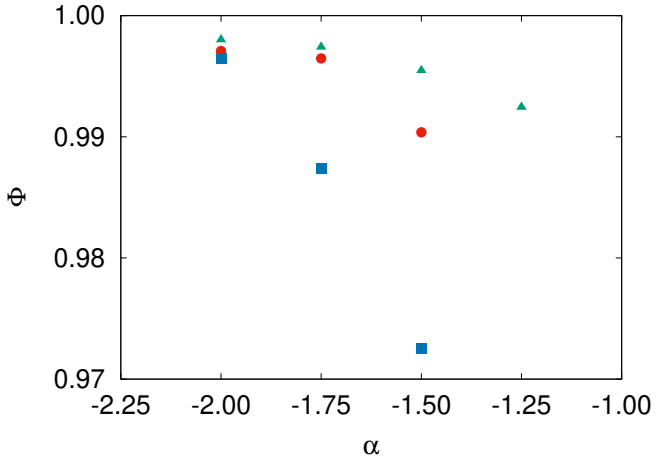

FIG. 5: Mean value of the vortex order parameter Φ as a function of α for $R = 16\Lambda$ (green triangles), $R = 23\Lambda$ (red circles), $R = 31\Lambda$ (blue squares).

RADIAL PROFILES OF THE GIANT VORTEX

The time-averaged, mean radial vorticity profile of the giant vortex $\overline{\omega}(r) = \frac{1}{2\pi r}\int \omega(\boldsymbol{r}')\delta(|\boldsymbol{r}'|-r)d^2r'$ displays a power law behavior $\overline{\omega}(r) \propto 1/r$ in the region $\Lambda \lesssim r \lesssim R - \Lambda$ far from the boundaries and from the center (Figure 6). A theoretical prediction for $\overline{\omega}(r)$ can be derived by assuming that the radial component of the velocity vanishes, $u_r = 0$, and that the angular component depends only on r as $u_\varphi = r\Omega(r)$, where $\Omega(r)$ is the angular velocity. The resulting vorticity field is $\omega = \boldsymbol{\nabla} \times \boldsymbol{u} = 2\Omega(r) + r\partial_r\Omega(r)$. Inserting these expressions in the equation for the vorticity, which is obtained by taking the curl of Eq. (1), and imposing the stationarity condition, one gets the following equation for $\Omega(r)$

$$(\alpha + \Gamma_2\nabla^2 + \Gamma_4\nabla^4)(2\Omega + r\partial_r\Omega) + \beta r^2\Omega^2(4\Omega + 3r\partial_r\Omega) = 0\ . \tag{2}$$

With the further assumption (justified a posteriori [58]) that the Swift-Hohenberg term is negligible for $r \gg \Lambda$, Eq. (2), admits the power-law solution $\Omega(r) = cr^\gamma$ with $c = \pm\sqrt{-\alpha/\beta}$ and $\gamma = -1$. This gives a prediction for the radial profiles of velocity $\overline{\boldsymbol{u}}(r) = \pm U\hat{\boldsymbol{\varphi}}$ and vorticity $\overline{\omega}(r) = \pm U/r$, which is in perfect agreement with our numerical findings (see Figure 6).

Beside the giant vortex, Figure 1 also shows the presence of vorticity fluctuations in an annular region close to the boundary. These have the aspect of elongated structures, slightly leaned in the direction of the mean flow of the

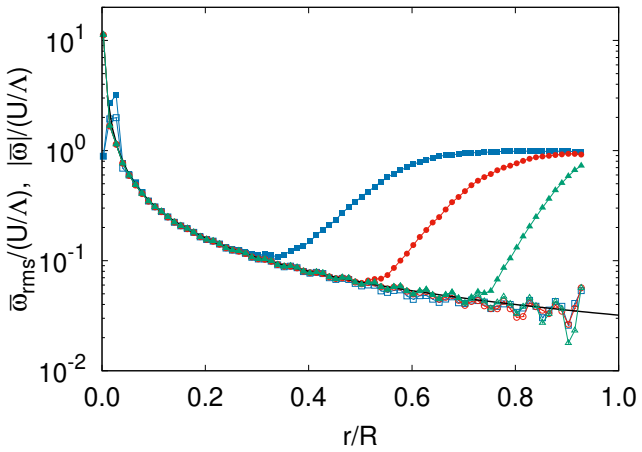

FIG. 6: Radial profiles of the vorticity, $\overline{\omega}(r)$ (empty symbols), and of the RMS vorticity, $\overline{\omega}_{rms}(r)$ (filled symbols), for simulations with $R = 31\Lambda$, $\alpha = -1.5$ (blue squares), $\alpha = -1.75$ (red circles) and $\alpha = -2$ (green triangles). The black line is the prediction $|\overline{\omega}(r)| = U/r$.

vortex, which extend from the boundary toward the center of the domain. These structures are composed by pairs of vortical streaks with opposite sign, corresponding to radial velocity jets with a typical transverse width of the order of Λ. The average number of streaks in a domain of radius R is therefore $N \simeq 2R\sqrt{\Gamma_2/2\Gamma_4}$. The formation of alternated streaks in the TTSH model has been observed also in numerical simulations in the absence of boundaries [37], and it is responsible for superdiffusive behavior of Lagrangian tracers [59].

The intensity of the vorticity fluctuations can be quantified by the RMS vorticity profile $\overline{\omega}_{rms}(r) = (\overline{\omega^2}(r))^{1/2}$ which is shown in Figure 6. Vorticity fluctuations are absent in the central region of the vortex in which $\overline{\omega}_{rms}(r)$ coincides with the mean radial profile $|\overline{\omega}(r)|$. They appear at larger r, as shown by the increase of $\overline{\omega}_{rms}(r)$ which reaches an almost constant plateau close to the boundary $\overline{\omega}_{rms}(r) \simeq U/\Lambda$.

Further details on the statistics of the streaks are revealed by the profiles of radial and angular velocity fluctuations defined as $\overline{u'_r}(r) = (\overline{u_r^2}(r))^{1/2}$ and $\overline{u'_\varphi}(r) = (\overline{u_\varphi^2}(r) - \overline{u_\varphi}^2(r))^{1/2}$, shown in Figure 7. The radial component is predominant in the velocity field of the streaks. Close to the boundary, the ratio between the intensities of radial and angular fluctuations is almost constant $\overline{u'_r}/\overline{u'_\varphi} \simeq 4.2$. The intensity of velocity fluctuations decays at increasing the distance from the boundary $R - r$.

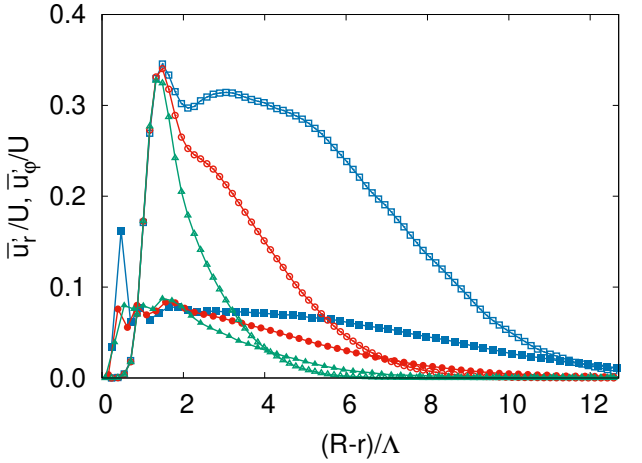

FIG. 7: Radial profiles of the radial and tangential components of the velocity fluctuations, $\overline{u'_r}(r)$ (empty symbols) and $\overline{u'_\varphi}((r)$ (filled symbols), as a function of the distance from the boundary for $\alpha = -1.75$, $R = 31\Lambda$ (blue squares), $\alpha = -1.5$, $R = 23\Lambda$ (red circles) and $\alpha = -1.25$, $R = 16\Lambda$ (green triangles).

The width of the region in which the streaks are present can be quantified as the distance δ from the boundary

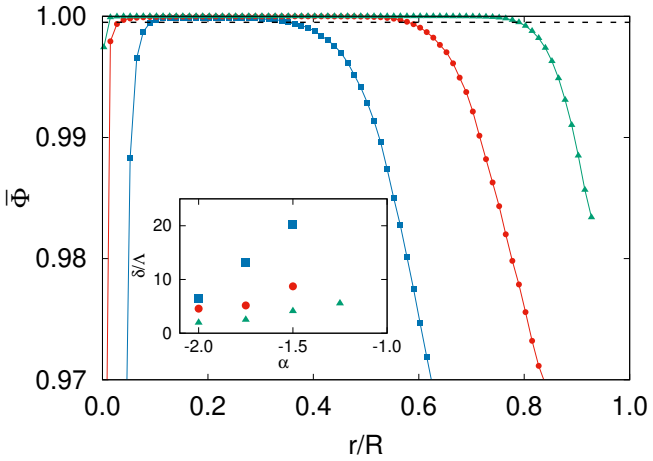

FIG. 8: Radial profiles of the vortex order parameter, $\overline{\Phi}(r)$, for simulations with $R = 31\Lambda$, $\alpha = -1.5$ (blue squares), $\alpha = -1.75$ (red circles) and $\alpha = -2$ (green triangles). The black dashed line is the threshold value $\Phi_{thr} = 0.9995$ used to define the width δ of the region in which the streaks are present. Inset: Width δ of the annular regions of the streaks as a function of α for $R = 16\Lambda$ (green triangles), $R = 23\Lambda$ (red circles), $R = 31\Lambda$ (blue squares).

at which the radial profile of the order parameter exceeds a given threshold value $\overline{\Phi}(R - \delta) = \Phi_{thr}$ (see Fig. 8). The values of δ (with $\Phi_{thr} = 0.9995$) are reported in the inset of Figure 8. We find that δ increases monotonically increasing the radius R of the circular domain and decreasing the parameter $|\alpha|$. The scaling of δ as a function of the parameters of the model and of the radius R remains an open question which deserves further theoretical studies.

DISCUSSIONS

The formation of the giant vortex surrounded by streaks is the results of competing mechanisms which can be understood by the comparison with the phenomenology observed in numerical simulations with periodic boundary conditions. In the latter case, the Landau potential and the self-propulsion term promote the development of a flocking state, in which all the bacteria swim in the same direction with a constant speed [47]. This collective ordered motion is destabilized by the Swift-Hohenberg operator which causes the formation of vorticity streaks in the transverse direction with respect to the mean flow [21]. A possible explanation of our findings is that the confinement in circular domains drives the system toward a state of circular flocking and then stabilizes it, preventing the formation of streaks in the center of the giant vortex. Vorticity fluctuations are nonetheless generated close to the boundary by friction forces. The vorticity production triggers the symmetry breaking of the angular momentum and facilitates the formation of the giant vortex.

Despite this simple interpretation, the formation of the giant vortex, is a highly non-trivial process which is far from being fully understood. As shown in Figure 1, the final state with a single vortex is achieved after a long turbulent regime in which several large-scale vortices compete with each other to prevail. We observed a strong variability of the duration of this intermediate regime for different realizations of the flow, which confirms the complexity of this process and suggests that the transition to the giant vortex may have a stochastic nature, with a broad distribution of the transition times.

We remark that the phenomenon presented here differs deeply from those previously reported in experiments [5, 43] and numerical simulations [45] of confined bacterial suspensions. The confining scale in these studies is much smaller than in our case, and the rectified vortex originates directly from the linear instabilities of the steady, no-flow state. Moreover, they found a double vortex with a non-monotonic radial profile of the azimuthal velocity [45], Conversely, the giant vortex observed in our study displays a uniform profile of azimuthal velocity surrounded by an annular region of vorticity streaks and it is produced by a non-linear mechanism from the interaction of the chaotic flow with the boundaries. This process requires a domain large enough to allow for the development of the turbulent-like regime which precedes the transition to the giant vortex. Our simulations show that a domain with radius $R = 16\Lambda$ is sufficient for this purpose.

The exact determination of the range of values of R/Λ in which the giant vortex forms remains an open question.

At fixed α we find that there is a maximum size of the domain which allows for the formation of the giant vortex. Nonetheless, it is extremely difficult to determine the precise value of this maximum size, because of the strong variability of the transition times. For values of R close to the maximum size, we observed the formation a giant vortex whose core consists of a binary rotating system of two small, equal-sign vortices (see Fig.9). Increasing further the radius R the evolution of the system remains in the turbulent regime characterized by multiple large-scale vortices which fail to merge in a single vortex during the simulation time.

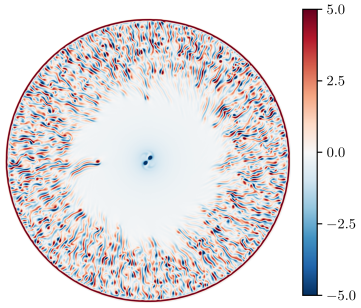

FIG. 9: Vorticity field in late stage of the simulation with $R = 31\Lambda$ and $\alpha = -1.50$, which displays a giant vortex whose core consists of a binary rotating system of two small, equal-sign vortices.

A comparison of the results of numerical simulations of the TTSH model and experiments of bacterial turbulence in confined geometry could shed new insight on this puzzling phenomenon. A quantitative correspondence between our simulations and a feasible experimental setup can be established by matching the parameters of the TTSH model with the typical values of the characteristic scale Λ and velocity U of the collective bacterial motion which are observed in experiments (e.g., in [4, 12, 26]). As an example, by fixing $\Lambda \simeq 25\mu m$ and $U \simeq 50\mu m/s$ the values of the radius R of the circular domain considered in our study correspond in physical units to the range $R \simeq (400 - 800)\mu m$, the values of the parameter α are in the range $-\alpha \simeq (1.4 - 1.8)s^{-1}$ and the typical time required to observe the formation of the giant vortex is of the order of minutes (see Figure 2). These spatial and temporal scales are easily accessible in experiments of dense bacterial suspensions, such as those of *Bacillus subtilis*.

ACKNOWLEDGMENTS

We acknowledges support from the Departments of Excellence grant (MIUR) and INFN22-FieldTurb. We thank M. Cencini for useful comments and suggestions.

* Corresponding author; stefano.musacchio@unito.it

[1] M. C. Marchetti, J.-F. Joanny, S. Ramaswamy, T. B. Liverpool, J. Prost, M. Rao, and R. A. Simha, Rev. Mod. Phys. **85**, 1143 (2013).
[2] S. Ramaswamy, Annu. Rev. Condens. Matter Phys. **1**, 323 (2010).
[3] R. Alert, J. Casademunt, and J.-F. Joanny, Annu. Rev. Condens. Matter Phys. **13** (2021).
[4] A. Sokolov and I. S. Aranson, Phys. Rev. Lett. **109**, 248109 (2012).
[5] H. Wioland, F. G. Woodhouse, J. Dunkel, J. O. Kessler, and R. E. Goldstein, Phys. Rev. Lett. **110**, 268102 (2013).
[6] C. Dombrowski, L. Cisneros, S. Chatkaew, R. E. Goldstein, and J. O. Kessler, Phys. Rev. Lett. **93**, 098103 (2004).
[7] A. Sokolov, R. E. Goldstein, F. I. Feldchtein, and I. S. Aranson, Phys. Rev. E **80**, 031903 (2009).
[8] A. Creppy, O. Praud, X. Druart, P. L. Kohnke, and F. Plouraboué, Phys. Rev. E **92**, 032722 (2015).
[9] F. Peruani, J. Starruß, V. Jakovljevic, L. Søgaard-Andersen, A. Deutsch, and M. Bär, Phys. Rev. Lett. **108**, 098102 (2012).
[10] Z. Liu, W. Zeng, X. Ma, and X. Cheng, Soft Matter **17**, 10806 (2021).
[11] A. Sokolov, I. S. Aranson, J. O. Kessler, and R. E. Goldstein, Phys. Rev. Lett. **98**, 158102 (2007).
[12] H. H. Wensink, J. Dunkel, S. Heidenreich, K. Drescher, R. E. Goldstein, H. Löwen, and J. M. Yeomans, Proc. Natl. Acad. Sci. U.S.A. **109**, 14308 (2012).
[13] A. P. Petroff, X.-L. Wu, and A. Libchaber, Phys. Rev. Lett. **114**, 158102 (2015).
[14] D. Nishiguchi, K. H. Nagai, H. Chaté, and M. Sano, Phys. Rev. E **95**, 020601 (2017).
[15] A. Morozov and D. Marenduzzo, Soft Matter **10**, 2748 (2014).

[16] G. Ariel, A. Rabani, S. Benisty, J. D. Partridge, R. M. Harshey, and A. Be'Er, Nat. Commun. **6**, 1 (2015).
[17] R. A. Simha and S. Ramaswamy, Phys. Rev. Lett. **89**, 058101 (2002).
[18] D. Saintillan and M. J. Shelley, Phys. Rev. Lett. **100**, 178103 (2008).
[19] A. Baskaran and M. C. Marchetti, Proc. Natl. Acad. Sci. U. S. A. **106**, 15567 (2009).
[20] A. Peshkov, I. S. Aranson, E. Bertin, H. Chaté, and F. Ginelli, Phys. Rev. Lett. **109**, 268701 (2012).
[21] J. Dunkel, S. Heidenreich, M. Bär, and R. E. Goldstein, New J. Phys. **15**, 045016 (2013).
[22] J. Słomka and J. Dunkel, Eur. Phys. J.: Spec. Top. **224**, 1349 (2015).
[23] S. Zhou, A. Sokolov, O. D. Lavrentovich, and I. S. Aranson, Proc. Natl. Acad. Sci. U. S. A. **111**, 1265 (2014).
[24] M. Bär, R. Großmann, S. Heidenreich, and F. Peruani, Annu. Rev. Condens. Matter Phys. **11**, 441 (2020).
[25] M. R. Shaebani, A. Wysocki, R. G. Winkler, G. Gompper, and H. Rieger, Nat. Rev. Phys. **2**, 181 (2020).
[26] J. Dunkel, S. Heidenreich, K. Drescher, H. H. Wensink, M. Bär, and R. E. Goldstein, Phys. Rev. Lett. **110**, 228102 (2013).
[27] G. Ariel, M. Sidortsov, S. D. Ryan, S. Heidenreich, M. Bär, and A. Be'Er, Phys. Rev. E **98**, 032415 (2018).
[28] H. Reinken, D. Nishiguchi, S. Heidenreich, A. Sokolov, M. Bär, S. H. Klapp, and I. S. Aranson, Commun. Phys. **3**, 1 (2020).
[29] F. Bonelli, G. Gonnella, A. Tiribocchi, and D. Marenduzzo, Eur. Phys. J. E **39**, 1 (2016).
[30] M. G. Giordano, F. Bonelli, L. N. Carenza, G. Gonnella, and G. Negro, EPL (Europhysics Letters) **133**, 58004 (2021).
[31] V. Bratanov, F. Jenko, and E. Frey, Proc. Natl. Acad. Sci. U. S. A. **112**, 15048 (2015).
[32] M. James and M. Wilczek, Eur. Phys. J. E **41**, 1 (2018).
[33] M. Linkmann, G. Boffetta, M. C. Marchetti, and B. Eckhardt, Phys. Rev. Lett. **122**, 214503 (2019).
[34] L. N. Carenza, L. Biferale, and G. Gonnella, Phys. Rev. Fluids **5**, 011302 (2020).
[35] V. M. Worlitzer, G. Ariel, A. Be'er, H. Stark, M. Bär, and S. Heidenreich, New J. Phys. **23**, 033012 (2021).
[36] V. M. Worlitzer, G. Ariel, A. Be'er, H. Stark, M. Bär, and S. Heidenreich, Soft Matter **17**, 10447 (2021).
[37] S. Mukherjee, R. K. Singh, M. James, and S. S. Ray, Phys. Rev. Lett. **127**, 118001 (2021).
[38] H. Wioland, E. Lushi, and R. E. Goldstein, New J. Phys. **18**, 075002 (2016).
[39] K.-T. Wu, J. B. Hishamunda, D. T. Chen, S. J. DeCamp, Y.-W. Chang, A. Fernández-Nieves, S. Fraden, and Z. Dogic, Science **355**, eaal1979 (2017).
[40] A. Doostmohammadi and J. M. Yeomans, Eur. Phys. J. Spec. Top. **227**, 2401 (2019).
[41] D. Nishiguchi, I. S. Aranson, A. Snezhko, and A. Sokolov, Nat. Commun. **9**, 1 (2018).
[42] A. Opathalage, M. M. Norton, M. P. Juniper, B. Langeslay, S. A. Aghvami, S. Fraden, and Z. Dogic, Proc. Natl. Acad. Sci. U. S. A. **116**, 4788 (2019).
[43] E. Lushi, H. Wioland, and R. E. Goldstein, Proc. Natl. Acad. Sci. U. S. A. **111**, 9733 (2014).
[44] K. Beppu, Z. Izri, J. Gohya, K. Eto, M. Ichikawa, and Y. T. Maeda, Soft Matter **13**, 5038 (2017).
[45] M. Theillard, R. Alonso-Matilla, and D. Saintillan, Soft Matter **13**, 363 (2017).
[46] J. Swift and P. C. Hohenberg, Phys. Rev. A **15**, 319 (1977).
[47] J. Toner and Y. Tu, Phys. Rev. Lett. **75**, 4326 (1995).
[48] J. Toner, Y. Tu, and S. Ramaswamy, Annals of Physics **318**, 170 (2005).
[49] M. James, D. A. Suchla, J. Dunkel, and M. Wilczek, Nat. Commun. **12**, 1 (2021).
[50] H. Reinken, S. Heidenreich, M. Bär, and S. H. Klapp, Phys. Rev. Lett. **128**, 048004 (2022).
[51] K. V. Kiran, A. Gupta, A. K. Verma, and R. Pandit, arXiv preprint arXiv:2201.12722 (2022).
[52] C. P. Sanjay and A. Joy, Phys. Rev. E **105**, 065114 (2022).
[53] S. Heidenreich, J. Dunkel, S. H. Klapp, and M. Bär, Phys. Rev. E **94**, 020601 (2016).
[54] H. Reinken, S. H. Klapp, M. Bär, and S. Heidenreich, Phys. Rev. E **97**, 022613 (2018).
[55] P. Angot, C.-H. Bruneau, and P. Fabrie, Numerische Mathematik **81**, 497 (1999).
[56] S. Liu, S. Shankar, M. C. Marchetti, and Y. Wu, Nature **590**, 80 (2021).
[57] S. Mukherjee, R. K. Singh, M. James, and S. S. Ray, arXiv preprint arXiv:2207.12227 (2022).
[58] The Swift-Hohenberg operator applied to a vorticity field $\overline{\omega}(r) = \pm U/r$ gives subleading terms of order $O((r/\Lambda)^{-3})$ which are negligible for $r \gg \Lambda$.
[59] R. K. Singh, S. Mukherjee, and S. S. Ray, Phys. Rev. Fluids **7**, 033101 (2022).